In situ observations of the "preexisting auroral arc" by THEMIS all sky imagers and the FAST spacecraft

Feifei Jiang,[1] Robert J. Strangeway,[1] Margaret G. Kivelson,[1,2] James M. Weygand,[1] Raymond J. Walker,[1] Krishan K. Khurana,[1] Yukitoshi Nishimura,[3] Vassilis Angelopoulos,[1] and Eric Donovan[4]

Received 6 September 2011; revised 25 January 2012; accepted 6 March 2012; published 5 May 2012.

[1] Auroral substorms were first described more than 40 years ago, and their atmospheric and magnetospheric signatures have been investigated extensively. However, because magnetic mapping from the ionosphere to the equator is uncertain especially during active times, the magnetospheric source regions of the substorm-associated features in the upper atmosphere remain poorly understood. In optical images, auroral substorms always involve brightening followed by poleward expansion of a discrete auroral arc. The arc that brightens is usually the most equatorward of several auroral arcs that remain quiescent for ~30 min or more before the break-up commences. In order to identify the magnetospheric region that is magnetically conjugate to this preexisting arc, we combine auroral images from ground-based imagers, magnetic field and particle data from low-altitude spacecraft, and maps of field-aligned currents based on ground magnetometer arrays. We surveyed data from the THEMIS all sky imager (ASI) array and the FAST spacecraft from 2007 to April 2009 and obtained 5 events in which the low altitude FAST spacecraft crossed magnetic flux tubes linked to a preexisting auroral arc imaged by THEMIS ASI prior to substorm onset. The observations show that, in each of the five cases: 1) the precipitating electrons associated with the preexisting arc are accelerated by a field-aligned potential drop, with characteristic energy ranging from a few hundred eV to a few keV. 2) The preexisting arc is located 1°~2° poleward of the equatorward edge of the 1 keV electron plasma sheet in the ionosphere, and it maps to equatorial locations within the electron plasma sheet and tailward of its inner edge. 3) The preexisting arc is located at or very near the boundary between the Region 1 and Region 2 field-aligned currents. The localization relative to the Region 1/Region 2 current is confirmed by comparison with maps of field-aligned currents inferred from ground magnetometer data.

Citation: Jiang, F., R. J. Strangeway, M. G. Kivelson, J. M. Weygand, R. J. Walker, K. K. Khurana, Y. Nishimura, V. Angelopoulos, and E. Donovan (2012), In situ observations of the "preexisting auroral arc" by THEMIS all sky imagers and the FAST spacecraft, *J. Geophys. Res.*, *117*, A05211, doi:10.1029/2011JA017128.

1. Introduction

[2] Active auroras are the most spectacular phenomena seen in the polar skies. Although very dynamic, auroral emissions commonly evolve in a predictable manner. In describing the temporal evolution of the aurora, *Akasofu* [1964] introduced the concepts of an auroral substorm and of the substorm expansion phase, which has come to be understood as the auroral signature corresponding to the release of free energy in a magnetotail instability. Akasofu noted that prior to the start of the substorm, quiescent discrete arcs, narrow in latitude and extended in longitude, appear in the night sky. This quiescent phase terminates at the onset of the expansion phase, which is characterized by a sudden brightening of one of the longitudinally extended quiet arcs, followed by rapid poleward and longitudinal expansion of the region of bright emissions. Furthermore, Akasofu noted that the most equatorward quiet arc is often the first to brighten and expand poleward, westward and eastward. In contrast to *Akasofu* [1964], *Lyons et al.* [2002] found that sometimes, auroral break-up occurs along a new arc that forms equatorward of all preexisting growth phase arcs in the last few minutes prior to the beginning of the expansion phase.

[3] Further insight into the auroral substorm was added by *McPherron* [1970], who introduced the idea that the

[1]Department of Earth and Space Sciences, University of California, Los Angeles, California, USA.
[2]Department of Atmospheres, Oceans and Space Sciences, University of Michigan, Ann Arbor, Michigan, USA.
[3]Department of Atmospheric and Oceanic Sciences, University of California, Los Angeles, California, USA.
[4]Department of Physics and Astronomy, University of Calgary, Calgary, Alberta, Canada.

Copyright 2012 by the American Geophysical Union.
0148-0227/12/2011JA017128

quiescent period preceding the expansion phase is actually an integral part of the substorm with characteristic evolution of the magnetospheric and ionospheric currents. He named this precursor interval the growth phase. During the growth phase the preexisting arc is often observed to move slowly equatorward.

[4] Both before and during a substorm, emissions from auroral arcs are stimulated by precipitating electrons. Although it is widely accepted that the brightening of a preexisting quiet arc is a direct signature of the onset of the expansion phase of an auroral substorm, the magnetospheric source of the electrons that excite both the preexisting arc and the brightened arc is not well understood. The magnetospheric counterpart of the arc remains enigmatic largely because of the uncertainty of mapping along the magnetic field lines from the ionosphere to the magnetotail. Low-altitude spacecraft and ground optical observations have provided insight into the source region and particle properties of the preexisting arc. *Lui and Burrows* [1978] argued that the arc that brightens at onset is magnetically conjugate to the transition region between dipolar and highly stretched topologies (a region they termed the "night side cusp"). Using the CANOPUS array of scanning photometers and precipitating ion and electron data from DMSP, *Samson et al.* [1992] showed that the arc that brightens forms within the region of bright proton aurora. *Voronkov et al.* [2000], *Deehr and Lummerzheim* [2001], and others have used ground-based optical data to show that the arc that brightens is on field lines poleward of the peak in brightness of the proton aurora, but in most if not all cases is within the bright proton aurora. *Yahnin et al.* [1997] proposed that the most equatorward discrete arc is on field lines that map to the earthward edge of a region of weak neutral sheet Bz, or equivalently, to a region in the center of the plasma sheet where the radius of curvature of field lines is so small that 30 keV electrons behave nonadiabatically. *Donovan et al.* [2008] studied ground-based and in situ data of one substorm event and argued that in that case the onset arc mapped to a region between 7 and 8 R_E in the magnetotail. Combining CANOPUS with in situ FAST measurements, *Lessard et al.* [2007] showed that in a number of events, the arc that brightens (which they termed "the growth phase arc") is excited by inverted-V electron precipitation [*Frank and Ackerson*, 1971].

[5] Because the magnetospheric source region of the preexisting arc remains uncertain, with links to several different locations having been proposed, it is the objective of this study to constrain to some degree the region of the magnetosphere to which it links. Previous studies have proven that auroral studies benefit from combining ground optical observations with in situ data from low-altitude spacecraft flybys. Fortunately, the THEMIS mission [*Angelopoulos*, 2008, and references therein] has provided greatly enhanced optical imagery of the auroral ionosphere in conjunction with simultaneous nighttime satellite observations in the near-Earth equatorial plasma sheet. Furthermore, during the early portion of the THEMIS mission the FAST spacecraft was providing low altitude data. Consequently, in this study, we survey data from the THEMIS All Sky Imager (ASI) and select intervals during which the FAST spacecraft crosses the magnetic shell of the preexisting arc. We have examined data from 11/2007 to 03/2008 and 11/2008 to 03/2009, when the orbit of FAST was favorable for conjunctions with the THEMIS ground array, selecting passes during which FAST crossed a quiet arc shortly before it brightened at the start of an auroral substorm. The FAST measurements reveal the location of the arc relative to large scale field-aligned currents (FACs) flowing between the magnetosphere and the ionosphere and identify the characteristics of the electrons that excite the arc. Ground magnetometer arrays can be used to map the distribution of FACs over a large part of the auroral zone [*Weygand et al.*, 2011] and enables us to infer the location of the preexisting arc relative to Region 1 and Region 2 currents.

[6] In the next section, the data and methods used in this study are introduced. Five events in which FAST crossed the magnetic shell of a quiet arc were identified. In section 3, we describe in detail three events in which FAST crossed a preexisting arc before a substorm onset near local midnight, in the pre-midnight sector and in the post-midnight sector, respectively. Observational results for all five cases are summarized. Section 4 discusses the implication of our results and compares our work with previous studies.

2. Data and Event Selection

[7] The THEMIS ground-based imager array consists of 20 all-sky white light imagers distributed across North America from Greenland to Alaska. Each imager has a field of view (FOV) of 9 latitudinal degrees at 110 km altitude and takes auroral images every 3 s [*Donovan et al.*, 2006; *Mende et al.*, 2006]. The imagers cover a large section of the auroral zone with roughly one-kilometer resolution at zenith, providing global auroral observations and broad coverage of the ionospheric footprint of the night-side magnetosphere.

[8] The FAST satellite was launched in 1996 and operated until March 2009 [*Pfaff et al.*, 2001; *Harvey et al.*, 2001]. It carried a fluxgate magnetometer and 4 electrostatic analyzers that measure particles of energies from a few eV to ~30 keV, with the highest time resolution of ~0.5 s. The high-resolution optical data from ASI enable us to pin down the ionospheric location of the preexisting arc and FAST measurements provide the properties of the precipitating particles that cause the auroral emissions. The insight gained by combining the two data sets is considerably enhanced by using ground magnetometer array to characterize the FAC structure not only along the FAST trajectory but also across a large part of the auroral region.

[9] We surveyed THEMIS ASI and FAST data from 11/2007 to 03/2008 and from 11/2008 to 03/2009, looking for events in which FAST crossed a preexisting arc in the field of view of the THEMIS ASIs. We verified that the arc selected as the preexisting arc was the one that brightened and expanded poleward within ~5 to ~50 min following the FAST crossing. Events were retained in the data set only if there was extensive enough coverage of the preexisting arc (i.e., we required the arc to have been imaged by several imagers) and FAST measurements were available during the time of the arc crossing. In addition, we required the FAST crossings to occur during geomagnetically quiet times prior to substorm onset or during a substorm growth phase. Geomagnetic conditions were characterized by the AL index. For quiet times AL was required to be small in magnitude ($AL > -50$ nT), whereas for a substorm growth phase, AL

Table 1. List of Observations of a Preexisting Arc by FAST and THEMIS All Sky Imagers[a]

Case	Date	Time of Conjunction (UT)	Time of Auroral Breakup (UT)	FAST Orbit	FAST MLT	Characteristic Energy of the Electron Precipitation
1	31 Jan 2009	06:33:36	06:56:00	S, 50311	0.1	~300 eV
2	14 Feb 2008	05:56:36	06:04:24	N, 46351	21	~500 eV
3	27 Feb 2009	05:15:06	05:27:00	N, 50615	21.5	~1 keV
4	2 Feb 2008	06:50:48	07:40:00	S, 46216	1.7	~800 eV
5	19 Dec 2008	08:21:03	08:26:30	S, 49828	3.4	~7 keV

[a]The event selection criteria are described in section 2.

was required to decrease gradually before reaching a minimum or starting to drop sharply. We required the preexisting arc of interest to remain undisturbed without visible changes in morphology till the auroral brightening began. We found five events in total, and they are listed in Table 1. The UT, magnetic local time and characteristic energy of the electron precipitation associated with the arc are listed for each event.

[10] To link FAST to the auroral features observed concurrently, we used the Tsyganenko 96 magnetic field model [*Tsyganenko*, 1995] with solar wind data input to map the FAST spacecraft to the ionosphere (taken to lie on a shell 120 km above the ground, around 1.02 R_E). The solar wind data are from the ACE satellite, appropriately time shifted to the nose of the magnetopause [*Weimer et al.*, 2003]. This is unnecessary (we could have just used the IGRF) for our events where FAST was located in the northern hemisphere as its apogee was at an altitude of 4200 km, but is essential when FAST was located in the southern hemisphere. Uncertainty of mapping from the T96 model arises when FAST was located in the southern hemisphere, but it is small at the magnetic latitude of the preexisting arc. In the five cases we studied, even when FAST was located in the conjugate (southern) hemisphere, its mapped ionospheric footprint crossed the relevant auroral arc signatures in the white light images within a few seconds before/after its detector recorded signatures of precipitating electrons, thereby confirming the validity of the magnetic mapping.

[11] In addition to THEMIS ASI and the FAST spacecraft, we used ground magnetometer data to calculate currents vertical to the earth's surface in the ionosphere [*Weygand et al.*, 2011]. The ground magnetometer stations analyzed are spread across North America and Greenland and include the THEMIS, CANMOS, CARISMA, MACCS, and Greenland arrays. The approach to measuring vertical currents by using ground magnetometer arrays is known as the spherical elementary current system (SECS) method and is described by *Amm and Viljanen* [1999] and *Weygand et al.* [2011]. Essentially, the technique applies the Biot-Savart law to calculate the vertical current at each grid point of an ionospheric grid from the horizontal magnetic perturbations measured at the array of ground stations, and assume that the vertical currents represent FACs. In the latitudinal range of interest in the ionosphere (e.g., from ~50° to ~70° in geographic latitude), the angle between the earth's main field and the direction normal to the earth's surface ranges from ~15° to ~5°. Therefore, the assumption that the vertical currents represent FACs is valid. With 81 ground magnetometer stations and ~1000 grid points and assuming uniform conductivity, the relationship between the vertical current and magnetic field can be written in the form $\mathbf{A}\boldsymbol{I} = \boldsymbol{B}$, where $\boldsymbol{I}$ is the amplitude of the vertical current at individual grid points, $\boldsymbol{B}$ is the horizontal vector of magnetic field perturbations at individual stations, and $\mathbf{A}$ is a matrix containing the magnetic field resulting from placing a unit vertical current at each grid point. The problem requires solving underdetermined linear equations. Applying a singular value decomposition (SVD) technique, $\boldsymbol{I}$ can be solved for given $\mathbf{A}$ and $\boldsymbol{B}$. The computation is performed in the spherical coordinate system. The SECS method used in this study for determining ionospheric currents has been widely used. *Pulkkinen et al.* [2003] tested this method for the BEAR and IMAGE magnetometer arrays by investigating the differences between the modeled and measured magnetic fields at various stations. Their test demonstrated that the SECS method applied with SVD is reliable and stable and is not highly sensitive to relatively large gaps in magnetometer arrays. Thus, this method serves as an effective tool for characterizing the ionospheric FAC distribution over a large portion of the auroral ionosphere. It is of particular value in placing the inferred currents along the track of the FAST spacecraft into a global context.

3. Event Study

3.1. 31 January 2009

[12] Figures 1a–1e are five consecutive images of an auroral substorm acquired by four THEMIS ground imagers between 06:31:00 UT and 07:13:00 UT on 31 January 2009. From left to right, the respective ground stations (circles) are Inuvik (top), Whitehorse, Gillam and Sanikiluaq. Imaging from the stations in between was obscured by clouds. FAST flew through the southern auroral zone during this conjunction. Its trajectory as mapped to the northern hemisphere is indicated by the yellow dashed line and its footprints at the UTs of Figures 1a and 1b are indicated by yellow crosses. The wiggling of FAST trajectory results from the variation of solar wind quantities that are input parameters of the T96 model. The footprints of the THEMIS spacecraft A, D and E, also mapped to the ionosphere using the T96 model, are indicated by the blue, orange and red squares respectively. The THEMIS spacecraft data and the mapping of the footprints will be discussed in section 4. Prior to the auroral breakup, a diffuse band of aurora and multiple arcs were present in the FOV of the imagers. A thin, faint arc located at the poleward edge of the diffuse aurora was the preexisting arc of interest (Figure 1b). It was also the most equatorward arc and it extended across ~30° in longitude from Gillam to Sanikiluaq (The latitudinal extent corresponds to 2 h of MLT). The preexisting arc is identified by the three red asterisks in Figures 1b–1d. FAST encountered the preexisting arc at 06:33:36 UT (in Figure 1b, the footprint of FAST from the T96 mapping is located 0.5° poleward of the arc). The arc gradually intensified and began to brighten at

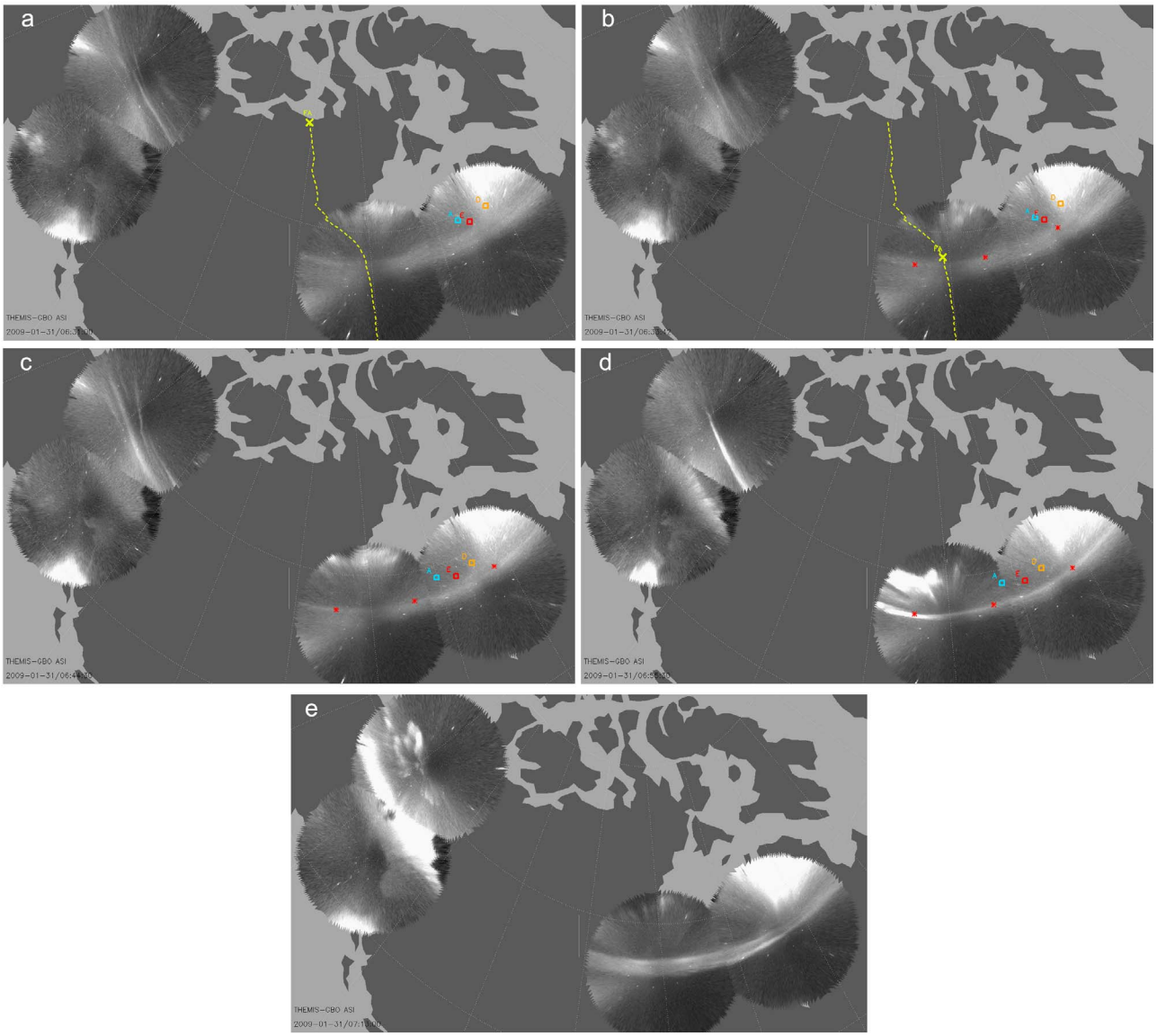

Figure 1. Snapshots of an auroral substorm on 31 January 2009 from THEMIS ASI. (a–e) The UTs are indicated at the bottom of the images. A substorm onset occurred at 06:55:30 UT. The trajectory and footprint of FAST are indicated by a yellow dotted line and a yellow cross, respectively on each image. In Figures 1b–1d, the preexisting arc is identified by red asterisks, and the footprints of THEMIS spacecraft A, D and E in the ionosphere are the blue, red and orange squares respectively.

06:55:30 UT (Figure 1d), and thereafter expanded (Figure 1e). An animation of ASI data for this event is shown in Animation S1 in the auxiliary material.[1] The track of the FAST spacecraft, mapped to the northern hemisphere, is shown moving equatorward and crossing the arc. The time evolution of the auroral substorm, including the gradual intensification and brightening of the preexisting arc, can be seen clearly in the animation.

[13] Figure 2 shows auroral indices versus UT from three hours before to two hours after the auroral brightening. The two vertical lines mark the time that FAST crossed the preexisting arc and the time of auroral brightening respectively. The first vertical line is located at a time when AL was −10 nT before it sharply dropped to −100 nT at 06:55 UT. It shows that FAST passed the preexisting arc during a geomagnetically quiescent time.

[14] Figure 3a shows the FAST data for a few minutes that include its passage across field lines that map to the preexisting arc. Panels from top to bottom are: energy flux spectrum versus energy (ranging from 4 eV to 30 keV) for electrons with a pitch angle range from 0° to 30°; energy flux spectrum versus energy for electrons with a pitch angle range from 60° to 120°; energy flux spectrum versus energy for electrons with a pitch angle range from 150° to 180°; ions omni-directional energy flux spectrum over an energy range from 4 eV to 25 keV; ions energy flux spectrum versus pitch angle for all energies; field-aligned ion fluxes integrated over an energy range from 1 keV to 25 keV; three

[1]Animations are available in the HTML.

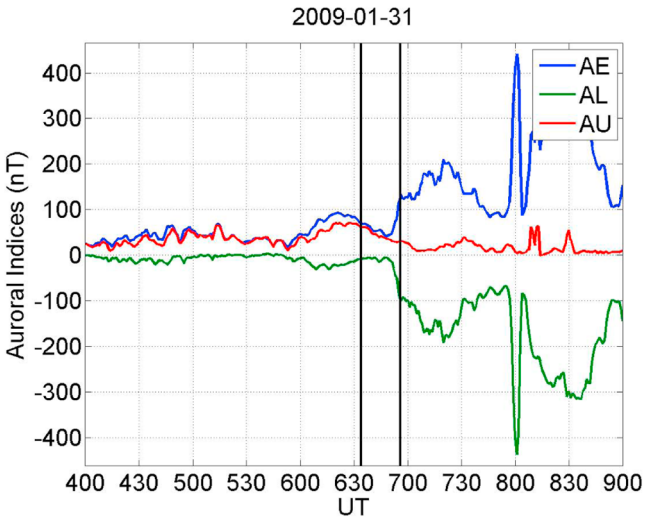

Figure 2. Auroral indices from 04:00 to 09:00 UT on 31 January 2009. AE, AL and AU are represented by blue, green and red respectively. The black vertical line near 06:30 UT indicates the time when FAST crossed the preexisting arc, and the black line near 07:00 UT indicates the time of auroral brightening.

components of the perturbed magnetic field in a field-aligned coordinate system; and amplitude of FAC density derived from magnetic field perturbations using Ampere's law (approximating curl-B by the change of cross-track perturbation with along-track distance). In the 6th panel, a negative value of the field-aligned ion flux indicates that it is anti-parallel to the background magnetic field and hence directed into the ionosphere in the southern hemisphere. In the 7th panel, the blue trace is the perturbed magnetic field component along the magnetic field (i.e., away from the earth for the southern hemisphere), the green trace is the east-west component of the perturbed magnetic field with positive direction to the east, and the red trace is the poleward component, with positive direction to the south in the southern hemisphere. The background magnetic field is given by the International Geophysical Reference Field (IGRF). The FAC density plotted in the 8th panel is calculated every 0.25 s (black trace), and the red trace is a 20-s running average of the black trace. A positive value of the FAC density indicates that it is parallel to the background magnetic field. In the southern hemisphere, positive FAC is out of the ionosphere, while negative FAC is into the ionosphere. The altitude, magnetic local time and invariant latitude of FAST are indicated at the bottom of the panels.

[15] Figure 3b illustrates the statistical distribution of large scale FACs in the ionosphere during weakly disturbed conditions [*Iijima and Potemra*, 1976, Figure 6]. The poleward portion of the large scale FACs are Region 1 currents, which flow into the ionosphere on the dawn side and out of the ionosphere on the dusk side. The Region 1 current system is believed to be associated with flow shear in the magnetopause boundary layers [*Lotko et al.*, 1987]. The large scale FACs equatorward of the Region 1 currents are Region 2 currents, which flow into the ionosphere on the dusk side and out of the ionosphere on the dawn side. The Region 2 current system is believed to be generated where the gradient of flux tube volume is not parallel to the gradient of plasma thermal pressure [*Vasyliunas*, 1972]. The red arrow in Figure 3b indicates the trajectory of FAST for this event, which flew through the auroral zone from pole to equator near local midnight, where the current configuration takes a more complicated three-sheet form. In individual cases, the actual distribution of large-scale field aligned currents is likely to differ from the statistical pattern in Figure 3b.

[16] In Figure 3a, the dashed magenta rectangle identifies the interval during which FAST observed precipitating electrons associated with the crossing of the preexisting arc shown in Figure 1b at 06:33:36 UT. At this time, the particle detector on FAST measured enhanced precipitating electron flux (3rd panel) which we take as the source of brightening even thought the T96 model, located the ionospheric footprint of FAST 0.5° north of the preexisting arc of interest (Figure 1b). The top panels show that the electron flux near 180° (3rd panel) at energies of a few hundred eV exceeds the flux at other pitch angles (1st and 2nd panels) in the same energy band, i.e., electrons are being accelerated into the southern ionosphere where FAST is located, evidence of a field-aligned potential drop. Within the FOV of the imagers, the arc marked by the asterisks is the only isolated discrete auroral arc that corresponds to the isolated electron precipitation structure at 06:33:36 UT. Therefore, it is the only plausible source of the preexisting arc. The narrow arc is excited by precipitating electrons accelerated by a field-aligned potential drop with a characteristic energy of ~300 eV. The equatorward boundary of the trapped electron flux (the gradual slope encountered almost a minute later from 06:34:30 UT to 06:35:00 UT in the 2nd panel of Figure 3a) is the inner edge of the trapped electron plasma

Figure 3. (a) FAST data including the arc crossing on 31 January 2009. Panels from top to bottom are: energy flux spectrum versus energy (ranging from 4 eV to 30 keV) for electrons with a pitch angle range from 0° to 30°; energy flux spectrum versus energy for electrons with a pitch angle range from 60° to 120°; energy flux spectrum versus energy for electrons with a pitch angle range from 150° to 180°; omni-directional ions energy flux spectrum; ions energy flux spectrum versus pitch angle for all energies; integrated field-aligned fluxes of ions over an energy range from 1 keV to 25 keV (black) and the average fluxes (red); components of the magnetic field perturbations in the field-aligned coordinate system: the blue trace is the perturbed magnetic field component along the magnetic field (away from the earth for the southern hemisphere), the green trace is the east-west component of the perturbed magnetic field with positive direction to the east, and the red trace is the poleward component, with positive direction to the south; FAC density derived from magnetic field perturbations (black) and averaged current density (red). The preexisting arc corresponds to the magenta dashed rectangle. (b) Illustration of the distribution of large-scale FACs in the ionosphere during weekly disturbed conditions [*Iijima and Potemra*, 1976, Figure 6]. The red arrow illustrates the trajectory of FAST for the pass shown in Figure 3a.

sheet. The energy-dependence of the inner edge can be understood as follows: In the equatorial plane, the inner edge of high energy plasma sheet electrons (~10 keV) lies outside of (at a larger radial distance) the inner edge of low energy plasma sheet electrons (~1 keV). Consequently, the equatorward boundary of ~10 keV plasma sheet electrons maps to a higher latitude than that of ~1 keV electrons. In Figure 3a, the preexisting arc is roughly 2° poleward of the inner edge of 1 keV electron plasma sheet, which maps to a source ~3 R_E displaced at the equator using the T96 model with real-time solar wind input. (We return to this argument in section 4.) The energy flux of ~1 keV – ~20 keV ions intensifies between ~68° and ~65° magnetic latitude (4th panel of Figure 3a), and the pitch angle distribution (5th panel) shows that the ions are precipitating. This enhanced ion precipitation is sometimes called the "proton

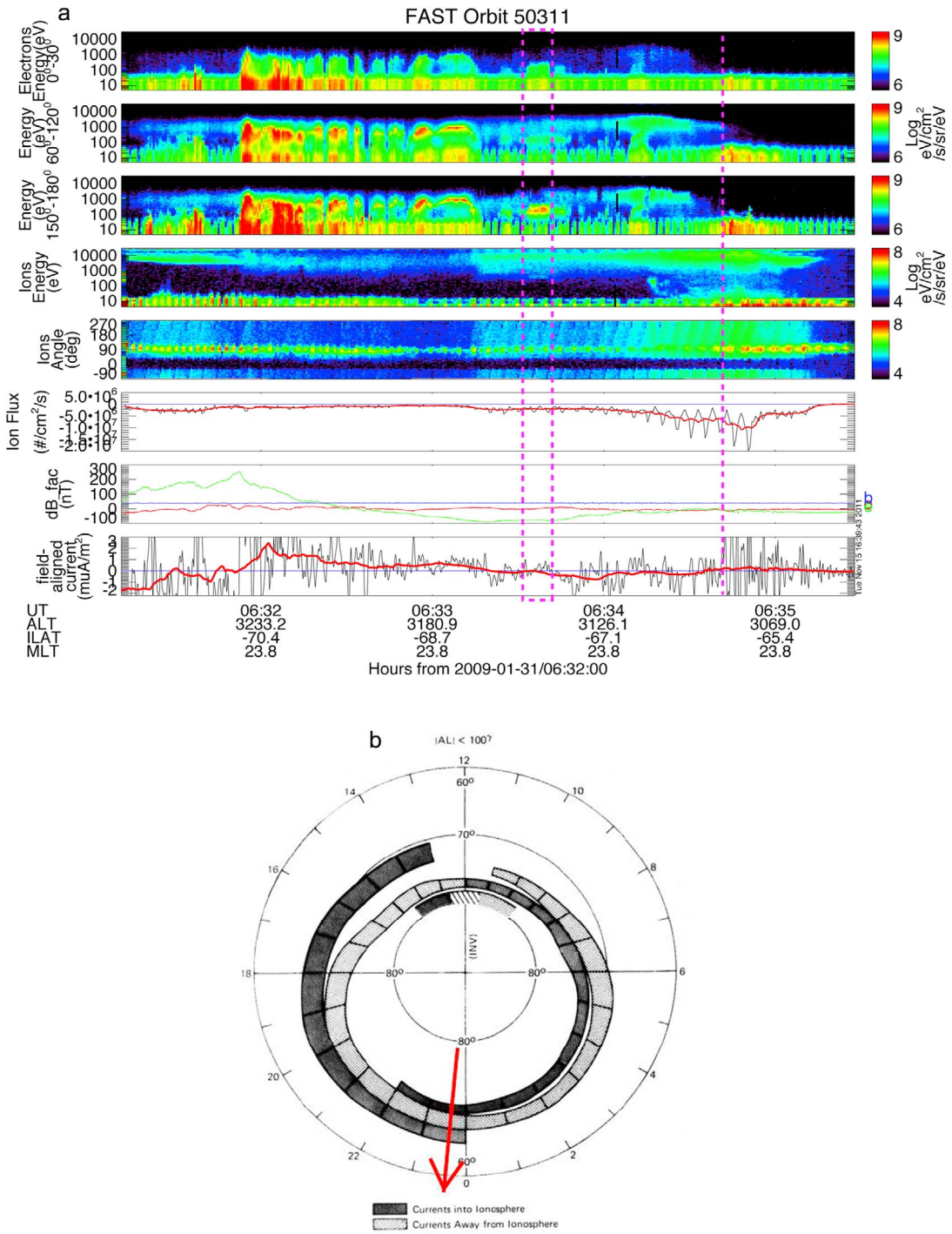

Figure 3

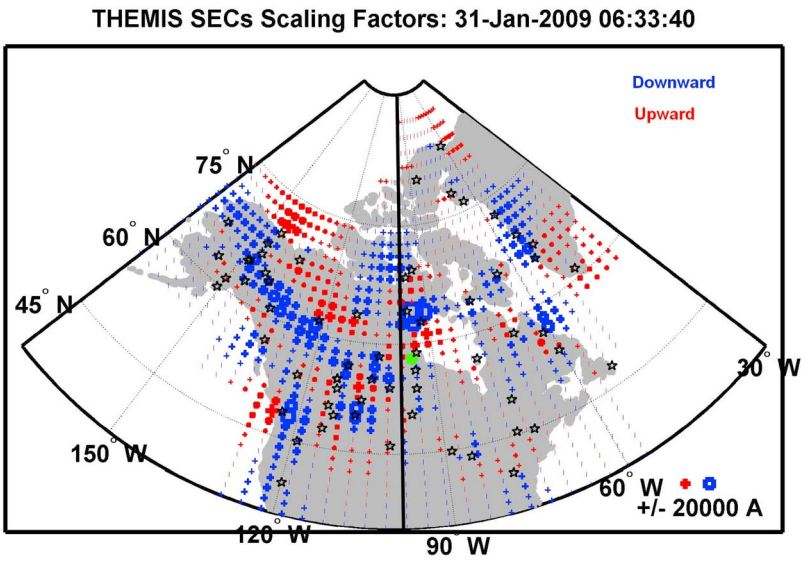

Figure 4. Distribution of vertical currents in the northern ionosphere at 06:33:40 on 31 January 2009, the time FAST encountered the preexisting arc. The vertical currents are determined from ground magnetometer data. Blue dots are downward vertical currents and red dots are upward vertical currents. The black line indicates magnetic midnight. The footprint of FAST at this time is marked by the green dot.

aurora." The peak of the precipitating ion fluxes is located at ~66° in invariant latitude and the preexisting electron arc is embedded within the "proton aurora," poleward of the peak precipitating fluxes. In the 7th panel, the east-west component of the perturbed magnetic field (green), is the dominant component of the magnetic perturbation measured by a spacecraft making a north-south cut through FAC sheets extended in longitude. The ascending slope of the eastward component of the magnetic field between 06:31:00 UT and 06:31:50 UT implies a region of downward FAC with magnitude of ~2 uA/m^2. The descending slope of the eastward component between 06:31:50 UT and 06:33:30 UT implies a region of upward FAC with amplitude around 1 uA/m^2. The much weaker ascending slope between 06:33:40 UT and 06:34:40 UT implies a region of downward FAC with amplitude around 0.5 uA/m^2. The jiggling in the east-west component of the magnetic field (green trace in the 7th panel) reflects localized structure in the FACs, as shown by the black trace in the 8th panel. Although multiple localized FAC structures exist, the overall trend of the magnetic field and the smoothed FAC density clearly show a net upward current embedded between two downward currents. The preexisting arc of interest is located at the boundary between the low-latitude Region 1 and Region 2 currents, appearing right after the westward component of the magnetic field reached a minimum.

[17] To further illustrate the relationship between the preexisting arc and the Region 1/Region 2 current system, we plot (Figure 4) the distribution of vertical currents in the northern ionosphere at 06:33:40 UT on 31 January 2009, the time FAST moved across the preexisting arc. The method used to make this plot was introduced in section 2. In Figure 4, the black stars represent ground magnetometer stations with good data. The blue squares and red "+" symbols are the current amplitudes calculated using the SECS method. The values are given in Figure 4 in units of amps and the direction is up or down with respect to the ionosphere. To get a good estimate of the FAC density from the SEC method the ionospheric electric field and height-integrated Hall and Pedersen conductivities are required. However, we can get a very rough estimate of the current density amplitude by dividing by the area (0.75 degrees geographic latitude by 1.75 degrees geographic longitude) surrounding the grid. The amplitude of the current ranges from −20000 to 20000 Ampere, implying that the current density is of order of 1 μA/m^2, a typical value for Region 1 and Region 2 FAC density. The larger the dot size, the larger the amplitude of current density. Magnetic midnight is marked by the black line. The distribution of the vertical currents is consistent with the statistical picture of the Region 1 and Region 2 FAC system (Figure 3b): in the pre-midnight sector, Region 1 currents are upward and Region 2 currents are downward; in the post-midnight sector, Region 1 currents are downward and Region 2 currents are upward. At midnight, the vertical current system becomes more complicated – an upward current sheet is located between two downward current sheets. The location of FAST at this time is marked by the green dot. Consistent with FAST data, the preexisting arc is located at the low-latitude edge of the outward field-aligned current produced by overlap of the pre-midnight and post-midnight R1/R2 current system. An animation of the distribution of the vertical currents plotted on top of the ASI for this event is shown in Animation S2. The red line indicates magnetic midnight, and the yellow star represents the footprint of FAST. The distribution of the upward and downward vertical currents remains relatively stable with time, and the preexisting arc is aligned with the boundary between the low-latitude pair of upward and downward FAC near local midnight (~58° in geographic latitude). The intensity of a pair of upward and downward

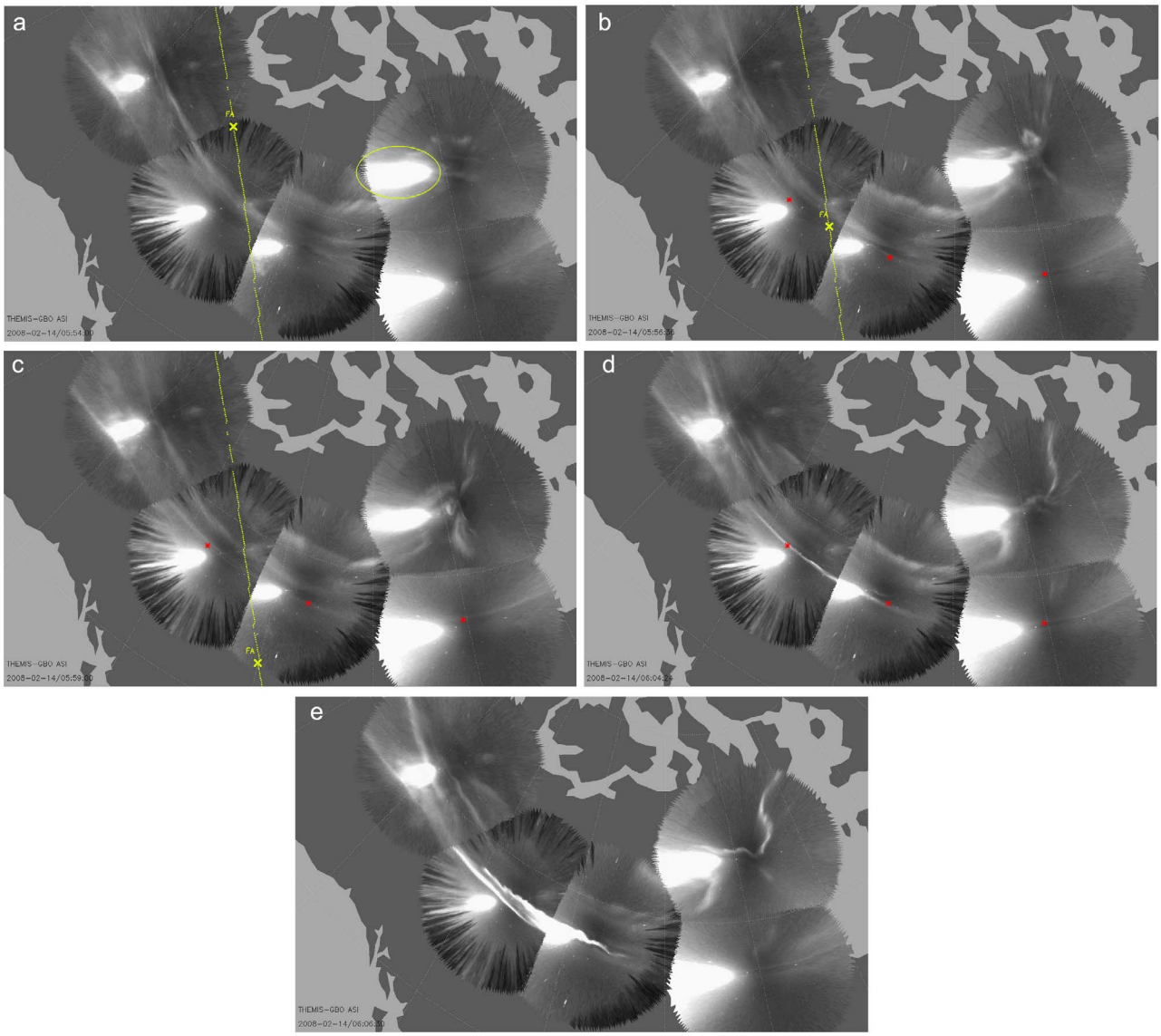

Figure 5. Snapshots of an auroral substorm on 14 February 2008 from THEMIS ASI. (a–e) The UTs are indicated at the bottom of the images. A substorm onset occurred at 06:04:24 UT. The trajectory and footprint of FAST are indicated by a yellow dotted line and a yellow cross. In Figures 5b–5d, the preexisting arc is identified by red asterisks.

currents near the preexisting arc increased at the substorm onset (06:55 UT).

3.2. 14 February 2008

[18] Figures 5a–5e are consecutive images of an auroral substorm acquired by five THEMIS ground imagers between 05:54:00 UT and 06:07:00 UT on 14 February 2008. The bright spot imaged at each station (marked by the yellow ellipse in the circles at the northeast) is moonlight. FAST flew through the northern auroral zone during this conjunction. Its trajectory as mapped to the northern hemisphere is indicated by the yellow dashed line and its footprints at the times (UT) corresponding to Figures 5a–5c are indicated by yellow crosses. Prior to the auroral breakup, several discrete arcs were present in the FOV of the imagers. The most equatorward one is a thin, faint arc that becomes visible (barely) in the image acquired as FAST crossed it at 05:56:36 UT (Figure 5b, in which the red crosses have been placed at several positions along the faint arc). It is imaged by 3 ASIs and extends roughly 40° in longitude (~3 h of MLT). The arc brightened at 06:04:24 UT (Figure 5d), and thereafter expanded poleward (Figure 5e). An animation of ASI data for this event is shown in Animation S3. Figure 6 shows the auroral indices versus UT from two hours before to two hours after the auroral brightening. The two vertical lines mark the time that FAST crossed the preexisting arc and the time of auroral brightening respectively. For this event, FAST encounter occurred during the late growth phase.

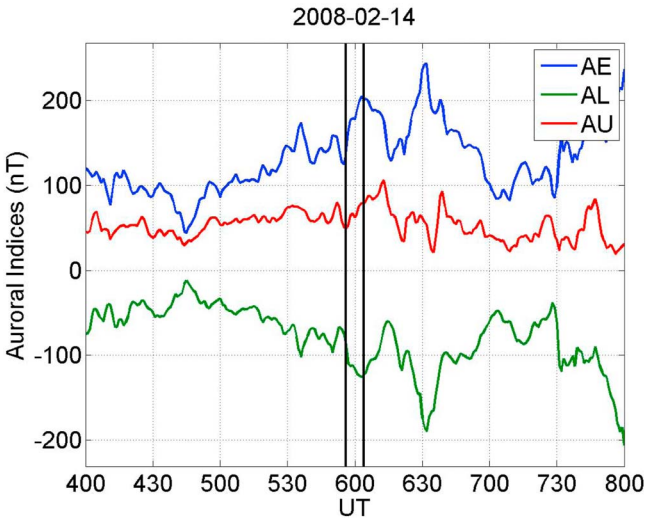

Figure 6. As for Figure 2, auroral indices from 04:00 to 08:00 UT on 14 February 2008. The black vertical line at 05:56 UT indicates the time FAST crossed the preexisting arc, and the black line at 06:04 UT indicates the time of auroral brightening.

[19] Figure 7a shows the FAST data for this event. Panels from top to bottom are the same as in Figure 3a. Figure 7b illustrates the trajectory of FAST relative to the large-scale FAC distribution. It shows that FAST flew through a two-sheet FAC layer in the pre-midnight sector (~2100 MLT) moving equatorward from high latitude. The dashed magenta rectangle in Figure 7a identifies the interval during which FAST, this time moving equatorward in the northern hemisphere, observed precipitating electrons associated with the crossing of the preexisting arc shown in Figure 5b at 05:56:36 UT. The flux of electrons with energy around a few hundred eV is greatly enhanced near 0° in pitch angle compared with that near 180° in pitch angle (1st and 3rd panel). This is indicative of a field-aligned potential drop of a few hundred eV that accelerates the electrons into the northern hemisphere. The arc is located 1° poleward of the inner edge of the 1 keV electron plasma sheet, which maps to a source ~1.5 R_E displaced at the equator using T96 model with concurrent solar wind input. Similar to event 1, the preexisting electron arc is embedded within the 1–20 keV ion precipitation and lies poleward of the peak precipitation. In the 7th panel, the positive slope of the eastward component of the magnetic field between 05:55 UT and 05:56:30 UT implies a region of upward FAC with magnitude of ~0.3 uA/m^2. The negative slope between 05:56:30 UT and 05:57:30 UT implies a region of downward FAC with amplitude of ~0.3 uA/m^2. Consistent with the statistical FAC distribution in the evening sector, the overall trend of the magnetic field and the smoothed FAC density shows an upward current layer lying poleward of a downward current layer. The preexisting arc of interest is located at the poleward edge of the Region 2 current, appearing right after the azimuthal component of the magnetic field reached a maximum.

[20] Figure 8 illustrates the distribution of vertical currents in the northern ionosphere at 05:56:36 UT on 14 February 2008, the time FAST moved across the preexisting arc. Magnetic midnight is marked by the black line. The location of FAST at this time is marked by the green dot. Consistent with the FAST data, the preexisting arc is located at the boundary between the upward Region 1 current and the downward Region 2 current. An animation of the time evolution of the distribution of the vertical currents for this event is shown in Animation S4. The red line indicates magnetic midnight, and the yellow star represents the FAST footprint. Once again in this event, the distribution of upward and downward currents remains relatively stable, and the preexisting arc is well aligned with the boundary between upward currents and downward currents in the pre-midnight sector. A slight increase in current density is seen at the preexisting arc (near 60°N) at substorm onset (06:04 UT).

3.3. 2 February 2008

[21] Figures 9a–9d are consecutive images of an auroral substorm acquired by 6 THEMIS ground imagers between 06:48:00 UT and 07:45:00 UT on 2 February 2008. FAST flew through the southern auroral zone during this conjunction. Its trajectory as mapped to the northern hemisphere is indicated by the yellow dashed line and its footprints at the times (UT) of Figures 9a and 9b are indicated by the yellow crosses. The ground station beneath the FAST footprint (SNKQ) was obscured by clouds and did not provide auroral images. However, the auroral features near the FAST footprint can be inferred from neighboring stations – GILL (the 2nd one on the right at the bottom) on the left of FAST and KUUJ (the 1st one on the right) on the right. Prior to the auroral breakup, multiple discrete arcs were present in the FOV of the imagers. At GILL, a bright discrete arc was located across the center of the image whereas at KUUJ, three discrete arcs were seen (Figure 9b). The bright discrete arc at GILL corresponds to the most poleward of the three (lowest latitude) discrete arcs at KUUJ and it brightens at substorm onset (Figure 9c) and expands afterwards. In this event, the quiet preexisting arc that brightened at substorm onset was not the most equatorward arc in the post-midnight sector (evident from KUUJ), but the most poleward one of the low-latitude arcs. The preexisting arc extends roughly 45° in longitude (3 h of MLT). Figure 9e plots the auroral intensity versus magnetic latitude at the central right meridian of GILL (~267° geographic longitude) at 06:51 UT. The highest peak at 66.7° corresponds to the brightest of the low-latitude preexisting arcs, whereas the two dashed magenta lines, marking local intensity peaks, correspond to the two arcs equatorward of the preexisting arc as seen at KUUJ. The time evolution of the auroral substorm for this event is shown in Animation S5. Figure 10 shows the auroral indices versus UT from two hours before to two hours after the auroral brightening. For this event, FAST crossed the arc during the early substorm growth phase.

[22] Figure 11a shows the FAST data for this event. Panels from top to bottom are the same as in Figure 3a. Figure 11b, analogous to Figure 3b, shows that FAST flew through a two-sheet FAC layer in the morning sector (0200 MLT) from the equator to the pole. The dashed magenta rectangle in Figure 11a identifies the interval during which FAST observed precipitating electrons (characteristic

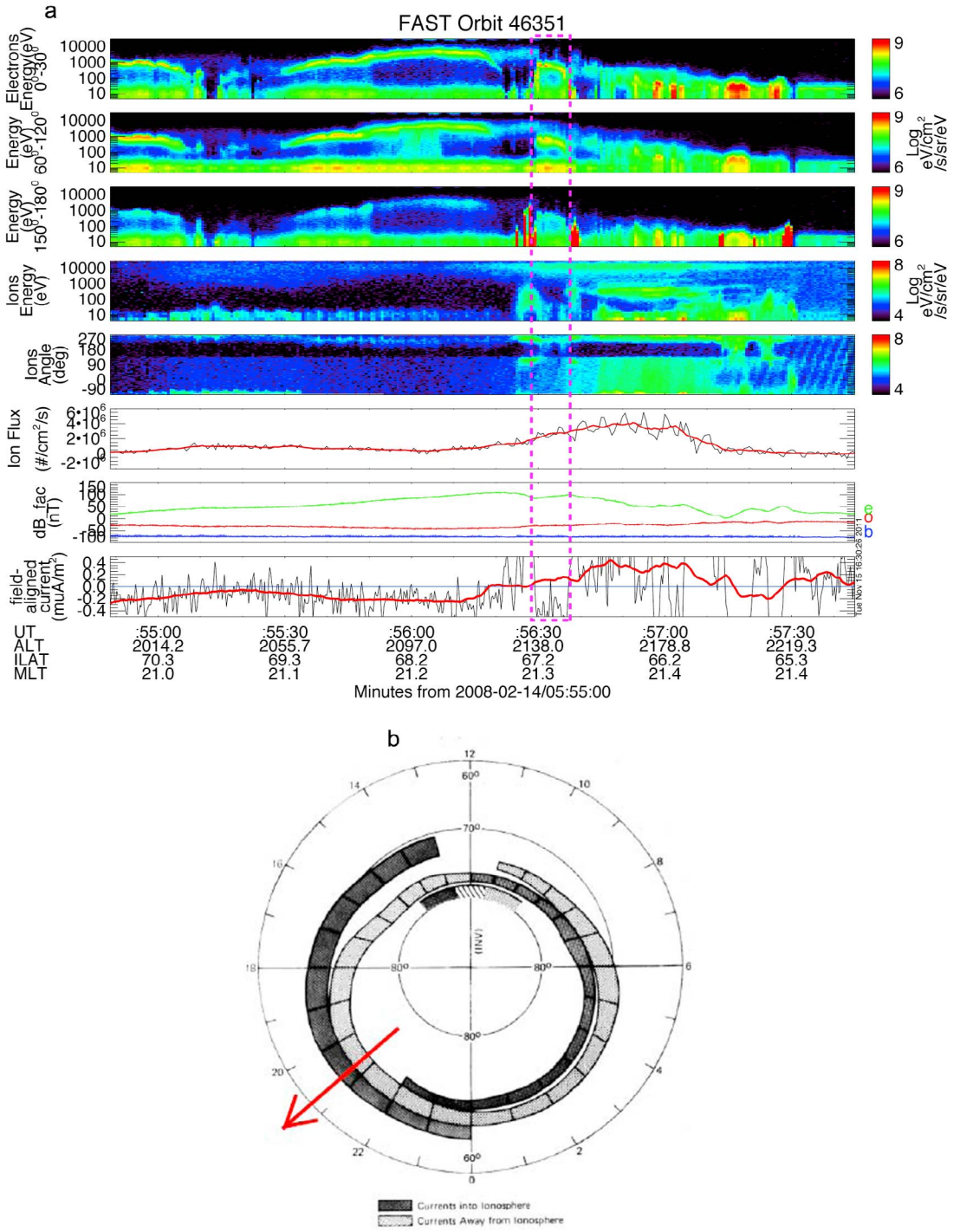

Figure 7. (a) FAST data including the arc crossing on 14 February 2008. Panels from top to bottom are the same as those in Figure 3a. (b) Illustration of the distribution of large-scale FACs in the ionosphere during weekly disturbed conditions. The red arrow illustrates the trajectory of FAST for the pass shown in Figure 7a.

energy slightly less than 1 keV) associated with the crossing of the preexisting arc shown in Figure 9b at 06:51:12 UT. This enhanced electron precipitation (centered at −66.5°) is very close in invariant latitude to the intensity peak at GILL (66.7°) and it is poleward of the energetic electron precipitation located from −65° to −66° (which corresponds to the diffused aurora equatorward of the preexisting arc at GILL). At about 06:51 UT, the electron energy spectrum near 180° in pitch angle shows enhanced fluxes with characteristic energy of ∼800 eV (3rd panel) and the precipitating

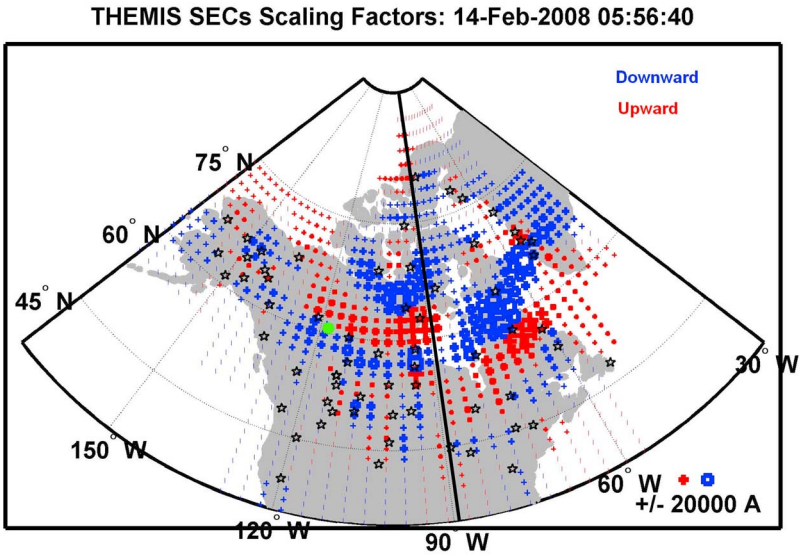

Figure 8. As in Figure 4, the distribution of vertical currents in the northern ionosphere at 0556:36 on 14 February 2008, the time FAST encountered the preexisting arc.

electron flux is much larger than the electron flux out of the ionosphere. This suggests a field-aligned potential drop of a few hundred eV above the FAST spacecraft that accelerates the electrons into the ionosphere. The inner edge of the electron plasma sheet is difficult to identify for this event due to the contamination of penetrating radiation flux (uniform flux enhancement across all the energy bins for both electrons and ions from 06:49 UT to 06:50 UT). The energetic ion precipitating fluxes (~1–~25 keV) have a peak at 06:50:30 UT and a poleward boundary at 06:51 UT. The preexisting electron arc is embedded within the ion precipitation and poleward of the peak precipitating fluxes. In the 7th panel, the positive slope of the eastward component of the magnetic field between 06:49 UT and 06:51:20 UT implies a region of upward FAC. The negative slope between 06:51:20 UT and 06:53 UT implies a region of downward FAC. The overall trend of the magnetic field and the smoothed FAC density shows a downward current layer lying poleward of an upward current layer. The preexisting arc is located at the poleward edge of the Region 2 current, appearing right before the azimuthal component of the magnetic field reached a maximum.

[23] Figure 12 illustrates the distribution of vertical currents in the northern ionosphere at 06:51:00 UT on 2 February 2008, the time FAST moved across the preexisting arc. The location of FAST is marked by the green dot. Consistent with the FAST data, the preexisting arc is located at the boundary between the upward Region 2 current and the downward Region 1 current. An animation of the time evolution of the distribution of vertical currents is shown in Animation S6. Again, the preexisting arc is aligned with the boundary between upward and downward currents, and the current intensity increases at substorm onset (07:41 UT).

[24] In the cases studied above, we find four distinct features of the preexisting arc: (1) the preexisting arc is embedded within the ~1 keV to ~20 keV ion precipitation and poleward of the most intense trapped and precipitating ion fluxes; (2) The preexisting arc is associated with precipitating electrons accelerated by a field-aligned potential drop, with characteristic energy ranging from a few hundred eV to 1 keV; (3) The preexisting arc is located ~1° to ~2° poleward of the inner edge of 1 keV electron plasma sheet in the ionosphere. For the cases where FAST crossed the pre-midnight auroral zone (events I and II), the latitudinal separation between the preexisting arc and the inner edge of 1 keV electron plasma sheet is ~1°. For the one case where FAST crossed the auroral zone at local midnight, the latitudinal separation between the preexisting arc and the inner edge of the 1 keV electron plasma sheet was 2°. For the one post-midnight passes where we are able to identify the inner edge (event 5), the latitudinal separation between the preexisting arc and inner edge of the 1 keV electron plasma sheet is ~1.4°. (4) The arc is located at or very near the interface between the Region 1 and Region 2 FAC: in the pre-midnight sector, the preexisting arc was located at the boundary between the downward Region 2 currents and upward Region 1 currents; in the post-midnight sector, the preexisting arc as located at the boundary between the upward Region 2 currents and downward Region 1 currents; near local midnight, the preexisting arc was located at the boundary between the low-latitude pair of FACs. Since the boundary between the R1 and R2 current systems is located at lower latitude on the evening side than on the morning side, the pre-midnight portion of the preexisting arc probably connects across the upward FAC region at local midnight, to the post-midnight portion of the arc. More passes in this region are needed to illuminate the preexisting arc's location relative to the large scale FAC system near local midnight.

4. Discussion and Conclusions

[25] From 5 FAST crossings of the clearly imaged growth-phase or quiescent "preexisting arcs" that brightened at substorm onset, we have found that the emissions are associated with precipitating electrons accelerated by a

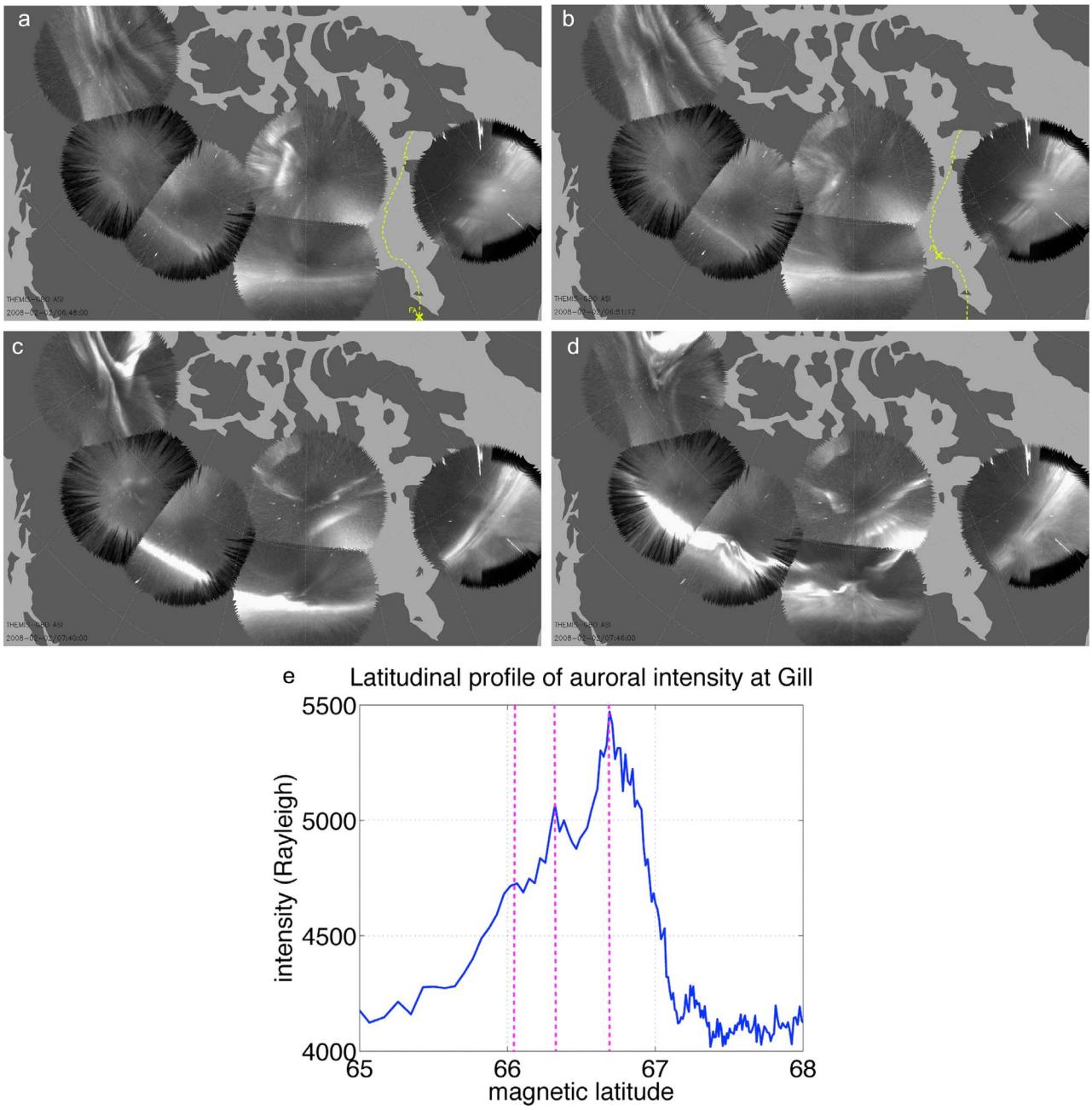

Figure 9. (a–d) Snapshots of an auroral substorm on 2 February 2008 from THEMIS ASI. The UTs of Figures 5a–5d are indicated at the bottom of the images. A substorm onset occurred at 07:40 UT. The trajectory and footprint of FAST are indicated by a yellow dotted line and a yellow cross. (e) Latitudinal profile of the auroral intensity in the meridian at ~267° in geographic longitude at GILL.

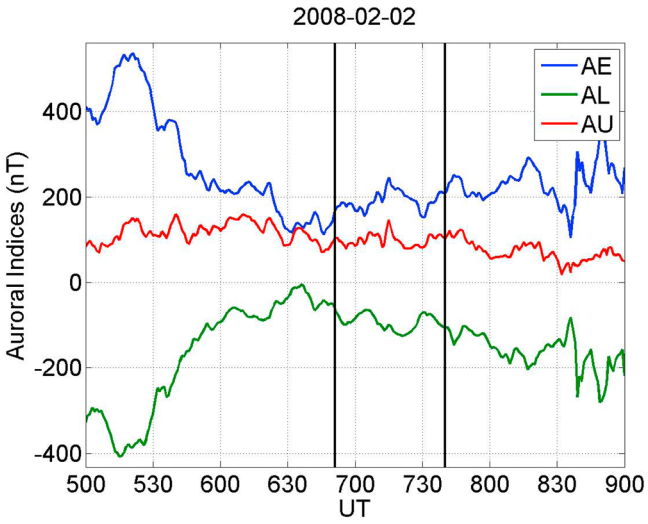

Figure 10. As for Figure 2, auroral indices from 05:00 to 09:00 UT on 2 February 2008. The black vertical line at 06:51 UT indicates the time FAST crossed the preexisting arc, and the black line at 07:40 UT indicates the time of auroral brightening.

field-aligned potential drop and are embedded within the energetic ion precipitation but poleward of the most intense ion precipitation. This result confirms previous studies regarding the location of the arc [e.g., *Jones et al.*, 1985; *Samson et al.*, 1992] and that the preexisting arc associated with precipitating electrons accelerated by field-aligned potential drops [*Lessard et al.*, 2007].

[26] *Ohtani et al.* [2010] used DMSP data to establish the location of various precipitation boundaries relative to Region 1 and Region 2 currents. They have found that in the dusk-to-midnight sector, the most equatorward "electron acceleration event" is often at the boundary between the Region 1 and Region 2 currents [*Ohtani et al.*, 2010, Figure 8]. Although *Ohtani et al.* [2010] did not survey any auroral image data in combination with DMSP and therefore could not distinguish "the preexisting arc" from an arbitrary electron acceleration event in the electron energy spectrum, their results are consistent with ours, in that the preexisting arc is often the equator-most discrete arc. In the midnight-to-dawn sector, however, our result differs from *Ohtani et al.* [2010]. They found that the most equatorward electron acceleration is in general within the Region 2 current [*Ohtani et al.*, 2010, Figure 8b] in the post-midnight region whereas in our event, the preexisting arc is located at the poleward boundary of the Region 2 currents.

[27] It is also of great interest to compare the characteristics of the "pre-existing arc" we found with those found for brightened onset arcs. *Shiokawa et al.* [2005] studied an event where the FAST spacecraft crossed several brightened auroral arcs after onset, and found that the most equatorward arc was located very near the equatorward boundary of the Region 1 current system. This is consistent with our observation and implied that the auroral arc remains at the boundary between the Region 1 and Region 2 FAC after the substorm onset is initiated. In addition, *Yago et al.* [2005] found that precipitating electrons associated with a pseudo-breakup arc corresponded to an electron inverted-V structure near the equatorward edge of the electron precipitation region, whereas *Mende et al.* [2003] examined FAST crossing of a substorm breakup arc one minute after onset and found that the onset arc was associated with highly intense wave-accelerated electrons. A statistical study by *Newell et al.* [2010] shows that precipitating power of broadband electron acceleration increases twice as much as that of mono-energetic electron acceleration after substorm onset. These results, in conjunction with our data, suggest that the precipitating electrons associated with the preexisting arc are mainly accelerated by field-aligned potential drops before onset, but that after the onset, both waves and field-aligned potential drops play a role in accelerating electrons into the ionosphere.

[28] The location of the preexisting arc relative to the inner edge of the electron plasma sheet in the ionosphere provides insight into its location in the magnetosphere. Since we have observed that the latitudinal separation between the preexisting arc and the inner edge is $\sim$1° to $\sim$2° at low altitude above the ionosphere from 2100 MLT to 0300 MLT, the preexisting arc map to a region a few R_E beyond the inner edge of the plasma sheet in this sector. The precise mapping into the magnetosphere is, however, quite uncertain, and here the concurrent THEMIS measurements can provide some constraints that we will next consider.

[29] *Jiang et al.* [2011] showed that the inner edge of the trapped electron plasma sheet is located in a dipolar region in the inner magnetosphere, at radial distances of 6–7 R_E from the Earth between 2200 and 0600 MLT during geomagnetically quiet times. This suggests that the preexisting arc could map to a radial distance of $\sim$10 R_E ($\sim$3 R_E away from the inner edge) or further tailward as a result of the stretched magnetic field configuration characteristic of the growth phase of a substorm. Figures 13a–13c show the magnetic field measured by THEMIS A, D and E located at radial distances of 10$\sim$11 R_E between 06:15 and 06:45 UT on 31 January 2009, for the event in Figure 1. The red curves represent the observed magnetic field whereas the blue curves represent the magnetic field calculated from the T96 model with solar wind input. Figure 13d displays the paths of THEMIS A, D and E in the GSM xy and xz planes during the half hour of interest. Around the time when FAST encountered the preexisting arc ($\sim$06:33 UT), the Bx component of the T96 modeled magnetic field was very close to that measured at THEMIS A, D and E, whereas the By and Bz components were off by a few nT. The discrepancy in the By component mainly shifts the footprint along the azimuthal direction whereas the discrepancy in the Bz component, which indicates that the model underestimates the field stretching, shifts the latitude of the footprint. In Figures 13a–13c, the modeled Bz component of the magnetic field is $\sim$5 nT larger than measured Bz component, almost a factor of 2 larger, indicating that the real magnetic field is much more stretched than predicted by the T96 model. This means that the ionospheric footprints of all three spacecraft must map to lower latitudes than those found using the T96 model. Since footprints of the THEMIS spacecraft obtained from the T96 model are located $\sim$1° poleward of the preexisting arc (Figure 1b), the actual footprints must be located very close to or even equatorward

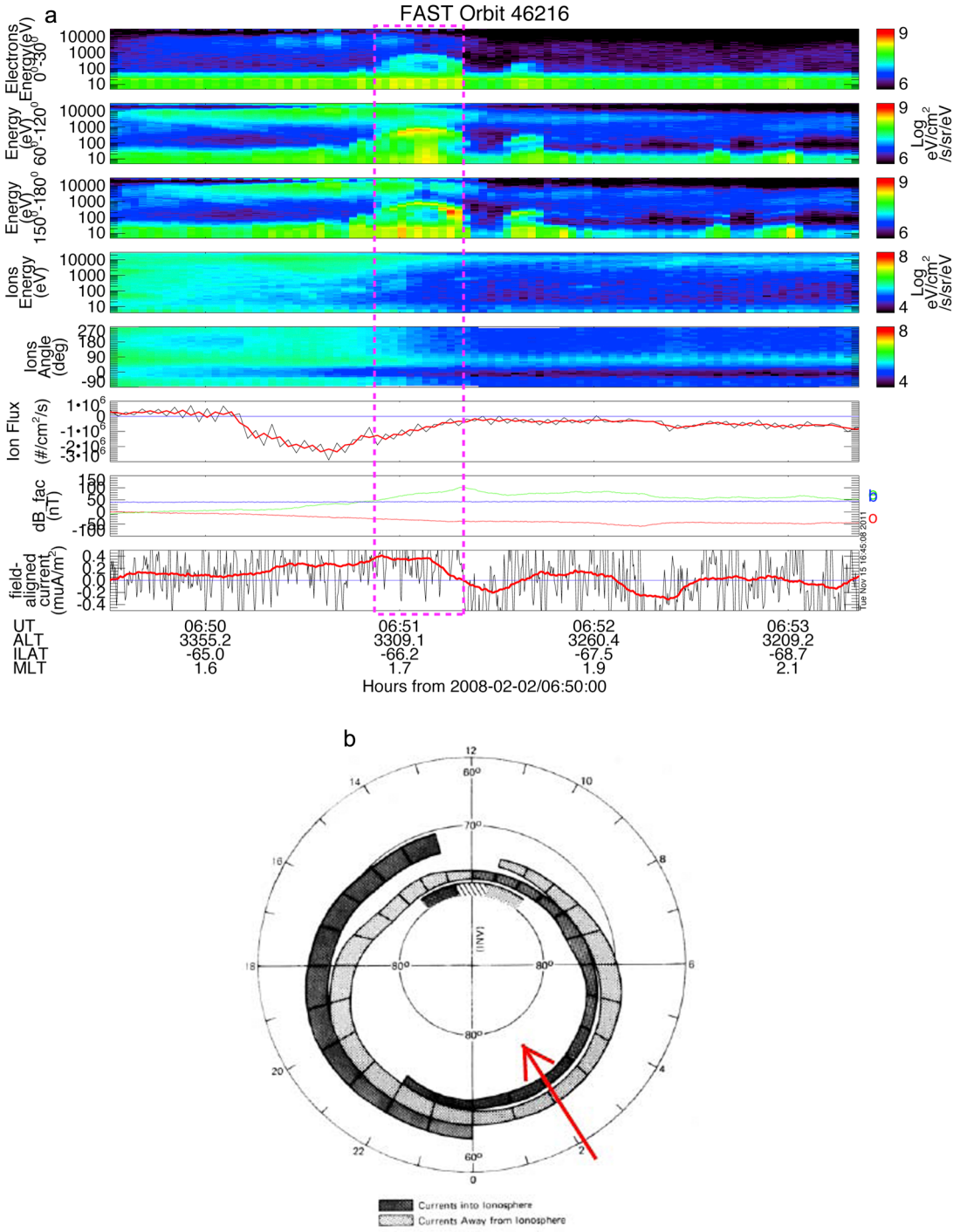

Figure 11. (a) FAST data including the arc crossing on 2 February 2008. Panels from top to bottom are the same as those in Figure 3a. (b) Illustration of the distribution of large-scale FACs in the ionosphere during weekly disturbed conditions. The red arrow illustrates the trajectory of FAST for the pass shown in Figure 11a.

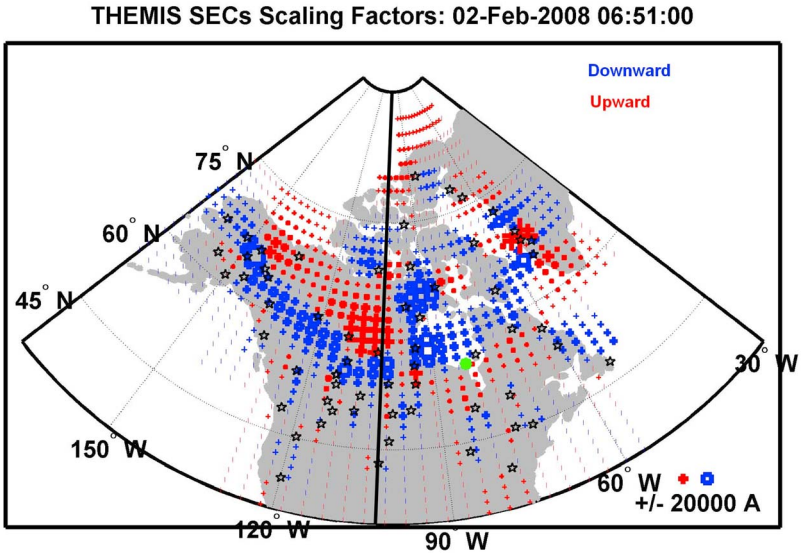

Figure 12. As in Figure 4, distribution of vertical currents in the northern ionosphere at 06:51:10 UT on 2 February 2008, the time when FAST encountered the preexisting arc.

of the arc. Plasma measurements on THEMIS D and E (not shown here) indicate that they were embedded within the electron plasma sheet and a few R_E away from the inner edge around this time. Therefore, the preexisting arc is very likely to be located in a region a few R_E beyond the inner edge. In addition, to test the shift of the spacecraft footprint in the ionosphere for a more realistic magnetic field configuration, we took the input variables of the T96 model (solar wind dynamic pressure, the Dst index, and the IMF By and Bz component) as free parameters, and looked for the values that minimize the variance between the modeled magnetic field and the observed magnetic field at THEMIS A, D and E. Consistent with the field stretching discussed above, the modified mapping with optimized input parameters puts the footprint very near the arc and poleward of the inner edge of the electron plasma sheet observed by FAST.

[30] We obtained similar mapping for the two additional cases listed in Table 1 in which the magnetic field was relatively undisturbed during the interval of interest and the mapped footprints were located within the FOV of the auroral imagers (case 2 and 3). In these cases once again, the T96 model significantly underestimates magnetic field stretching and correcting for this effect, the modified ionospheric footprints of THEMIS D and E (located around 10 R_E radially) are found to be located near or equatorward of the preexisting arc. For case 4 there were significant perturbations of the magnetic field during the time of interest and such temporal variation cannot be modeled or even approximated by the T96 model. For case 5 the footprints of the THEMIS spacecraft were located far outside of the FOV of auroral imagers. Thus, all cases for which estimated mapping is meaningful support the view that the preexisting arc maps to a source in the magnetosphere within the electron plasma sheet and tailward of its inner edge. Our mapping of the preexisting arc to the magnetosphere is also similar to that obtained by *Sergeev et al.* [2012]. However, they relate the magnetospheric source region of the preexisting arc to the isotropy boundary of 30—300 keV electrons caused by large field line curvature in the magnetotail whereas we relate it to a boundary of large-scale FACs of different polarities.

[31] To summarize, from a survey of THEMIS ground optical data as well as FAST data from 2007 to April 2009, we obtained 5 conjunction events where FAST crossed a growth-phase or quiescent "preexisting arcs" that remained visible and quiescent until it brightened within an hour at the time of a substorm onset. The arcs were imaged by multiple all-sky cameras and were found to extend over 2–3 h of MLT. The principal conclusions of our study are as follows: (1) We have confirmed that the precipitating electrons associated with the preexisting arc are accelerated by field-aligned potential drops; (2) We have found that in the ionosphere, the preexisting arc is located 1°∼2° in latitude poleward of the inner edge of the electron plasma sheet, and that it maps to a region tailward of the inner edge of the electron plasma sheet (6–7 R_E at the equator) in the magnetosphere. The radial separation is found to be ∼3 R_E using modified T96 model for our relatively undisturbed events. For a very stretched magnetic field configuration (such as that typical of the late growth phase), the radial separation can be much larger. Although there is considerable uncertainty in the mapping to the equator, it is of interest to note that these estimates suggest the arc links to an equatorial region near 8 to 10 R_E, with an azimuthal extent of at least 2–3 h (or equivalently >4 R_E in length). (3) We have shown that, for all the 5 conjunction events, the "preexisting arc" is located at or very near to the boundary between the Region 1 and Region 2 field-aligned currents, independent of the time between the FAST crossing and the time of auroral breakup. This finding constrains the magnetospheric region that is the source of both the preexisting arc and the arc that brightens at substorm onset. It would be interesting to learn how this observation can be incorporated into various models of substorms.

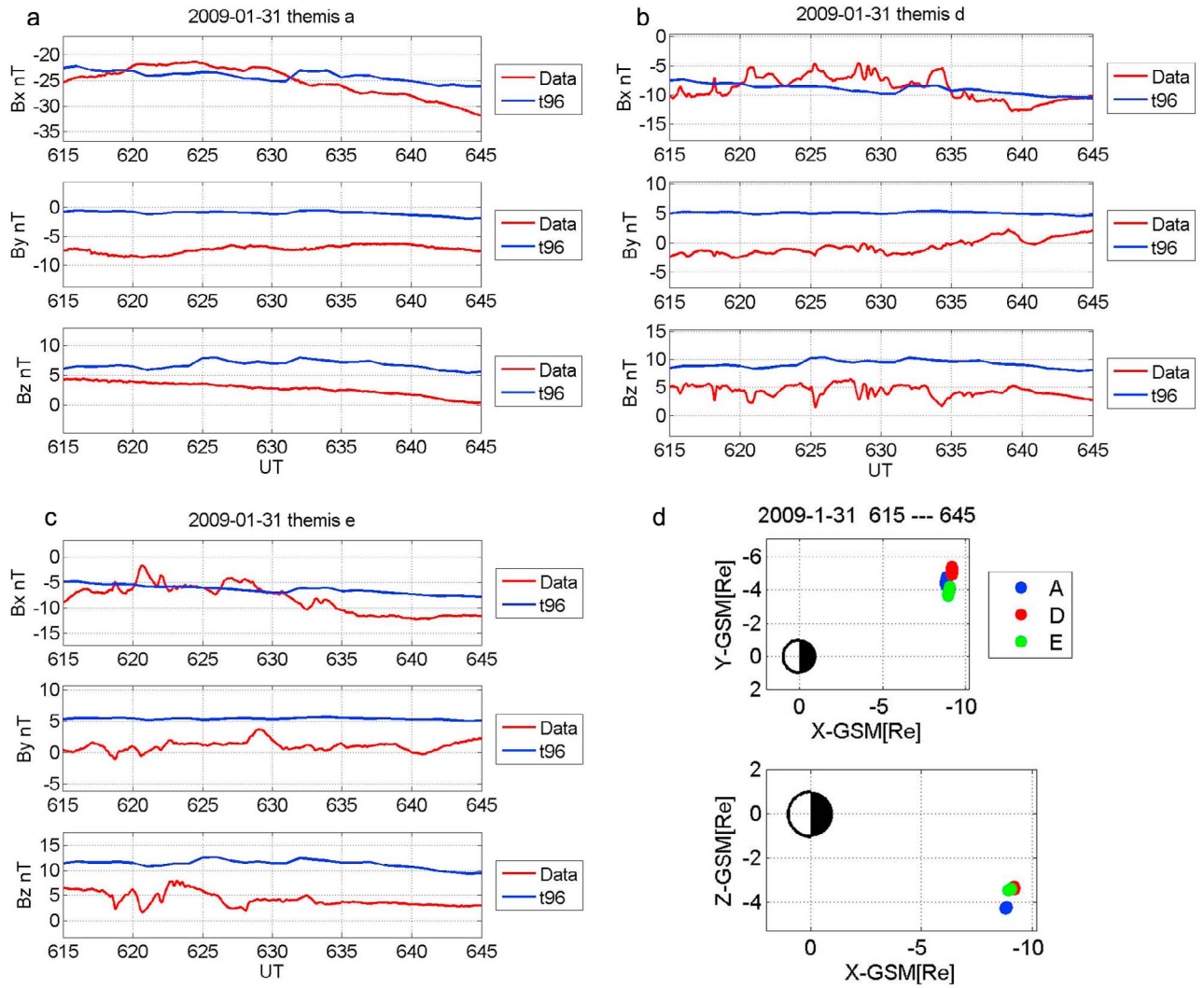

Figure 13. (a–c) Magnetic field at THEMIS A, D and E from 06:15 UT to 06:45 UT on 31 January 2009, for the event in Figure 1. The red curves are measured magnetic field whereas the blue curves are magnetic field calculated by the T96 model with real-time solar wind input. The radial distance and MLT of each spacecraft are indicated below the panels. (d) Trajectories of THEMIS A, D and E on the GSM xy and xz planes from 06:15 UT to 06:45 UT on 31 January 2009.

[32] **Acknowledgments.** This work was supported by the NASA THEMIS funding 443869-TM-22620. R. J. Strangeway was supported by NASA "Living With a Star" grant NNX07AT15G. Helpful suggestions from Dr. Robert McPherron are gratefully appreciated. THEMIS is made possible by NASA NAS5–02099. We thank S. Mende for use of the data from the ASI and U. Auster, K. H. Glassmeier and W. Baumjohann for use of the data from the FGM instrument. We acknowledge financial support for the THEMIS-ASI program from the Canadian Space Agency.

[33] Robert Lysak thanks the reviewers for their assistance in evaluating this paper.

References

Akasofu, S. I. (1964), The development of the auroral substorm, *Planet. Space Sci.*, *12*, 273–282, doi:10.1016/0032-0633(64)90151-5.

Amm, O., and A. Viljanen (1999), Ionospheric disturbance magnetic field continuation from the ground to the ionosphere using spherical elementary current systems, *Earth Planets Space*, *51*, 431–440.

Angelopoulos, V. (2008), The THEMIS mission, *Space Sci. Rev.*, *141*(1–4), 5–34.

Deehr, C., and D. Lummerzheim (2001), Ground-based optical observations of hydrogen emission in the auroral substorm, *J. Geophys. Res.*, *106*(A1), 33–44, doi:10.1029/2000JA002010.

Donovan, E., et al. (2006), The THEMIS all-sky imaging array—System design and initial results from the prototype imager, *J. Atmos. Sol. Terr. Phys.*, *68*, 1472–1487, doi:10.1016/j.jastp.2005.03.027.

Donovan, E., et al. (2008), Simultaneous THEMIS in situ and auroral observations of a small substorm, *Geophys. Res. Lett.*, *35*, L17S18, doi:10.1029/2008GL033794.

Frank, L. A., and K. L. Ackerson (1971), Observations of charged particle precipitation into the auroral zone, *J. Geophys. Res.*, *76*(16), 3612–3643, doi:10.1029/JA076i016p03612.

Harvey, P. R., D. W. Curtis, H. D. Heetderks, D. Pankow, J. M. Rauch-Leiba, S. K. Wittenbrock, and J. P. McFadden (2001), The FAST spacecraft instrument data processing unit, *Space Sci. Rev.*, *98*, 113–149, doi:10.1023/A:1013135809232.

Iijima, T., and T. Potemra (1976), Field-aligned currents in the dayside cusp observed by Triad, *J. Geophys. Res.*, *81*(34), 5971–5979, doi:10.1029/JA081i034p05971.

Jiang, F., M. G. Kivelson, R. J. Walker, K. K. Khurana, V. Angelopoulos, and T. Hsu (2011), A statistical study of the inner edge of the electron

plasma sheet and the net convection potential as a function of geomagnetic activity, *J. Geophys. Res.*, *116*, A06215, doi:10.1029/2010JA016179.
Jones, V., F. Creutzberg, R. L. Gattinger, and F. R. Harris (1985), Auroral studies with a chain of meridian scanning photometers 1. Observations of proton and electron aurora in magnetospheric substorms, *J. Geophys. Res.*, *87*(A6), 4489–4503, doi:10.1029/JA087iA06p04489.
Lessard, M. R., W. Lotko, J. LaBelle, W. Peria, C. W. Carlson, F. Creutzberg, and D. D. Wallis (2007), Ground and satellite observations of the evolution of growth phase auroral arcs, *J. Geophys. Res.*, *112*, A09304, doi:10.1029/2006JA011794.
Lotko, W., B. U. Ö. Sonnerup, and R. L. Lysak (1987), Nonsteady boundary layer flow including ionospheric drag and parallel electric fields, *J. Geophys. Res.*, *92*(A8), 8635–8648, doi:10.1029/JA092iA08p08635.
Lui, A. T. Y., and J. R. Burrows (1978), On the location of auroral arcs near substorm onsets, *J. Geophys. Res.*, *83*(A7), 3342–3348, doi:10.1029/JA083iA07p03342.
Lyons, L. R., I. O. Voronkov, E. F. Donovan, and E. Zesta (2002), Relation of substorm breakup arc to other growth-phase auroral arcs, *J. Geophys. Res.*, *107*(A11), 1390, doi:10.1029/2002JA009317.
McPherron, R. (1970), Growth phase of magnetospheric substorms, *J. Geophys. Res.*, *75*(28), 5592–5599, doi:10.1029/JA075i028p05592.
Mende, S. B., C. W. Carlson, H. U. Frey, L. M. Peticolas, and N. Østgaard (2003), FAST and IMAGE-FUV observations of a substorm onset, *J. Geophys. Res.*, *108*(A9), 1344, doi:10.1029/2002JA009787.
Mende, S. B., S. E. Harris, H. U. Frey, V. Angelopoulos, C. T. Russell, E. Donovan, B. Jackel, M. Greffen, and L. M. Peticolas (2006), The THEMIS array of ground-based observatories for the study of auroral substorms, *Space Sci. Rev.*, *141*(1–4), 357–387.
Newell, P. T., A. R. Lee, K. Liou, S.-I. Ohtani, T. Sotirelis, and S. Wing (2010), Substorm cycle dependence of various types of aurora, *J. Geophys. Res.*, *115*, A09226, doi:10.1029/2010JA015331.
Ohtani, S., S. Wing, P. T. Newell, and T. Higuchi (2010), Locations of night-side precipitation boundaries relative to R2 and R1 currents, *J. Geophys. Res.*, *115*, A10233, doi:10.1029/2010JA015444.
Pfaff, R., C. Carlson, J. Watzin, D. Everett, and T. Gruner (2001), An overview of the fast auroral snapshot (FAST) satellite, *Space Sci. Rev.*, *98*(1–2), 1–32, doi:10.1023/A:1013187826070.
Pulkkinen, A., O. Amm, and A. Viljanen (2003), Ionospheric equivalent current distributions determined with the method of spherical elementary current systems, *J. Geophys. Res.*, *108*(A2), 1053, doi:10.1029/2001JA005085.
Samson, J. C., L. R. Lyons, P. T. Newell, F. Creutzberg, and B. Xu (1992), Proton aurora and substorm intensifications, *Geophys. Res. Lett.*, *19*(21), 2167–2170, doi:10.1029/92GL02184.
Sergeev, V., Y. Nishimura, M. Kubyshkina, V. Angelopoulos, R. Nakamura, and H. Singer (2012), Magnetospheric location of the equatorward prebreakup arc, *J. Geophys. Res.*, *117*, A01212, doi:10.1029/2011JA017154.
Shiokawa, K., K. Yago, K. Yumoto, D. G. Baishev, S. I. Solovyev, F. J. Rich, and S. B. Mende (2005), Ground and satellite observations of substorm onset arcs, *J. Geophys. Res.*, *110*, A12225, doi:10.1029/2005JA011281.
Tsyganenko, N. (1995), Modeling the Earth's magnetospheric magnetic field confined within a realistic magnetopause, *J. Geophys. Res.*, *100*(A4), 5599–5612, doi:10.1029/94JA03193.
Vasyliunas, V. M. (1972), The interrelationship of magnetospheric processes, in *Earth's Magnetospheric Processes*, edited by B. M. McCormac, pp. 29–38, D. Reidel, Hingham, Mass., doi:10.1007/978-94-010-2896-7_3.
Voronkov, I., E. Donovan, B. Jackel, and J. Samson (2000), Large-scale vortex dynamics in the evening and midnight auroral zone: Observations and simulations, *J. Geophys. Res.*, *105*(A8), 18,505–18,518, doi:10.1029/1999JA000442.
Weimer, D. R., D. M. Ober, N. C. Maynard, M. R. Collier, D. J. McComas, N. F. Ness, C. W. Smith, and J. Watermann (2003), Predicting interplanetary magnetic field (IMF) propagation delay times using the minimum variance technique, *J. Geophys. Res.*, *108*(A1), 1026, doi:10.1029/2002JA009405.
Weygand, J. M., O. Amm, A. Viljanen, V. Angelopoulos, D. Murr, M. J. Engebretson, H. Gleisner, and I. Mann (2011), Application and validation of the spherical elementary currents systems technique for deriving ionospheric equivalent currents with the North American and Greenland ground magnetometer arrays, *J. Geophys. Res.*, *116*, A03305, doi:10.1029/2010JA016177.
Yago, K., K. Shiokawa, K. Hayashi, and K. Yumoto (2005), Auroral particles associated with a substorm brightening arc, *Geophys. Res. Lett.*, *32*, L06104, doi:10.1029/2004GL021894.
Yahnin, A. G., V. A. Sergeev, B. B. Gvozdevsky, and S. Vennerstrom (1997), Magnetospheric source region of discrete auroras inferred from their relationship with isotropy boundaries of energetic particles, *Ann. Geophys.*, *15*, 943–958, doi:10.1007/s00585-997-0943-z.

V. Angelopoulos, F. Jiang, K. K. Khurana, M. G. Kivelson, R. J. Strangeway, R. J. Walker, and J. M. Weygand, Department of Earth and Space Sciences, University of California, Los Angeles, CA 90095, USA. (fjiang@igpp.ucla.edu)
E. Donovan, Department of Physics and Astronomy, University of Calgary, Calgary, AB T2N 1N4, Canada.
Y. Nishimura, Department of Atmospheric and Oceanic Sciences, University of California, 405 Hilgard Ave., Los Angeles, CA 90095, USA.